Available online at www.sciencedirect.com

ScienceDirect

Transportation Research Procedia 70 (2023) 388–397

Transportation Research Procedia

www.elsevier.com/locate/procedia

8th International Electric Vehicle Conference (EVC 2023)

State-of-Charge Estimation of Li-ion Battery Packs Based on Optic Fibre Sensor Measurements

Shiyun Liu[a], Kang Li[a,*], Benjamin Chong[a], Ye Chen[b]

[a]*School of Electronic and Electrical Engineering, University of Leeds, LS2 9JT, UK*

[b]*School of Physics, Nanjing University of Aeronautics and Astronautics, No.29 Jiangjun Avenue, Jiangning District, Nanjing, China*

Abstract

This paper presents a battery pack State-of-Charge (SOC) estimation approach by integrating both the cell-based strategy and the pack-based strategy. The approach first utilizes an optic fibre sensor network to monitor variations in strain across the battery cells, based on which a strain model is developed to estimate the SOC of single cells. Then, the cell-based strategy is adopted, for which the SOC of a pack is determined by the highest SOC of single cells observed during charging and the lowest SOC of single cells during discharging. To improve the SOC estimation accuracy of the battery pack strategy, the Thevenin model is employed in conjunction with the Extended Kalman Filter (EKF). The final SOC estimation of the battery pack is then obtained by averaging the results obtained from both the cell-based strategy and the pack-based strategy. Experimental results confirm that this modelling strategy can significantly improve the estimation accuracy and reliability.

Keywords: Li-ion battery packs, SOC estimation, Optic Fibre sensor, Strain model, Kalman filter

1. Introduction

As an important battery state used in the battery management system (BMS), State of Charge (SOC) plays a vital role in maintaining cell balance and indicating the remaining capacity of the battery pack. However, estimating pack SOC can be challenging due to inconsistencies among the hundreds or thousands of cells within a pack. The existing battery pack SOC estimation methods can be categorized into the "Big cell" approach, "Representative Cell" approach, and "Each Cell" approach.

The "Big cell" approach considers the battery pack as a single large cell, and then various cell-based models are applied to estimate the overall pack SOC using parameters such as terminal voltage, current, and temperature (Yu et al., 2023). This approach incurs less calculation effort but the cell inconsistency across the pack is not considered, leading to a low estimation accuracy due to the existence of differences in the internal parameters between cells.

* Corresponding author.
E-mail address: K.Li1@leeds.ac.uk (K. Li), yechen@nuaa.edu.cn (Y. Chen)

2352-1465
10.1016/j.trpro.2023.11.044

Nomenclature

SOC	State-of-Charge
EKF	Extended Kalman Filter
FRA	Fast Recursive Algorithm
EMI	Electromagnetic interference
FBG	Fibre Bragg Grating
ECM	Equivalent Circuit Model
MSE	Mean squared error
MAE	Mean Absolute Error
CC-CV	Constant-Current Constant-Voltage
CC	Constant-Current
Ah	Ampere-hour

The "Representative cell" approach uses representative cells (SOC_{lower} and SOC_{upper}) to estimate the SOC of a battery pack. During the discharging process, the cell with the lowest voltage is used to indicate the SOC of the battery pack. While for the charging process, the cell with the highest voltage is used to indicate the SOC of the battery pack. This method can improve the safety of a battery pack, however, for battery packs commonly used in the 30% ~ 80% SOC operating range, it limits the full utilization of the energy capacity of a battery pack (Hua et al., 2015).

Unlike the "Big cell" approach, the "each cell" methods estimate the SOC of the battery pack by estimating the SOC of each cell (Dai et al., 2012). While this approach can produce a detailed map of cell SOC across the battery pack, it incurs a high wiring and computational cost.

All the existing approaches use electric signals to estimate the SOC of a battery pack, while electric signals are susceptible to electromagnetic interferences (EMI) in a hash environment, leading to poor estimations. In this work, we propose a strain-based method to produce high accurate battery pack SOC estimation. Firstly, optic fibers were installed on the surface of each in-pack cell to monitor surface strain changes. Then, the Fast Recursive Algorithm (FRA) method (Li and Peng, 2005) was used to establish the relationship between battery parameters and strain values. FRA selects the most important features based on the measurement signals of current, voltage, SOC, and temperature for each cell. Then, the strain model is coupled with the Extended Kalman Filter (EKF) to estimate the SOC of each cell. We further use the "big cell" strategy to estimate the overall battery pack SOC, based on which the final battery pack SOC was obtained by averaging the results obtained from both the cell-based strategy and the pack-based strategy.

2. Preliminary work

In order to enhance readability, this section will introduce the concepts of FRA and EKF, which are fundamental to the proposed estimation method. Additionally, the criteria for model evaluation will be presented in this section.

2.1. Fast Recursive Algorithm

Consider a nonlinear discrete-time dynamic system characterized by a linear-in-the-parameters model (Li et al., 2021), which is identified by N data samples $\{x(i), y(i)\}_{i=1}^{N}$

$$y = \Psi\Theta + \mathbf{E} \tag{1}$$

where $\mathbf{y} = [y(1), \ldots, y(N)]^T \in \Re^N$ represents the system output, $\mathbf{\Psi} = [\varphi_1, \ldots, \varphi_i, \ldots, \varphi_k] \in \mathbb{R}^{N\times k}$ is the regression matrix that contains all candidate model terms, each term $\varphi_i \in \Re^{N\times 1}, \varphi_i = [\varphi_i(x(1)), \ldots, \varphi_i(x(N))]^T$ $(i = 1, \ldots, k)$ represents a basis function with N samples, $\Theta = [\theta_1, \ldots, \theta_k]^T$ are the unknown parameters to be identified, and $\mathbf{E} = [\mathbf{e}_1, \ldots, \mathbf{e}_N]^T$ is the model residual vector.

The modelling purpose is to simultaneously choose the most significant model terms while identify the unknown parameters within the least squares framework where the cost function is defined as the sum of squared estimate of errors (SSE). To achieve this, two recursive matrices, namely information matrix $\mathbf{M}_k$ and residual matrix $\mathbf{R}_k$, are defined in FRA to fulfil the forward model term selection procedure:

$$\begin{cases} \boldsymbol{M}_k = \boldsymbol{\varphi}_k^T \boldsymbol{\varphi}_k, k-1, \ldots, n \\ \boldsymbol{R}_k = \boldsymbol{I} - \boldsymbol{\varphi}_k \boldsymbol{M}_k^{-1} \boldsymbol{\varphi}_k^T, R_0 = I \end{cases} \tag{2}$$

where $\boldsymbol{\Psi}_k \in \Re^{N \times k}$ contains the first k selected model terms of the full regression matrix. R_k has the following properties:

$$\boldsymbol{R}_k^T = \boldsymbol{R}_k, (\boldsymbol{R}_k)^2 = \boldsymbol{R}_k \tag{3}$$

$$\boldsymbol{R}_k \boldsymbol{R}_j = \boldsymbol{R}_j \boldsymbol{R}_k = \boldsymbol{R}_k, k \geqslant j \tag{4}$$

$$\boldsymbol{R}_k \varphi_i = 0, \forall i \in \{1, \ldots, k\} \tag{5}$$

$$\boldsymbol{R}_{k+1} = \boldsymbol{R}_k - \frac{\boldsymbol{R}_k \varphi_{k+1} \varphi_{k+1}^T \boldsymbol{R}_k^T}{\varphi_{k+1}^T \boldsymbol{R}_k \varphi_{k+1}}, k = 0, 1, \ldots, n-1 \tag{6}$$

Suppose E_k is the sum squared error after selecting k terms, and it can be expressed as

$$E_k = \boldsymbol{y}^T \boldsymbol{R}_k y \tag{7}$$

Based on Eq. (6) and Eq. (7), the cost function after adding the $(k+1)th$ term can be expressed as

$$\Delta E_{k+1} = -\frac{\left(y^T \varphi_{k+1}^{(k)}\right)^2}{\left(\left(\varphi_{k+1}^{(k)}\right)^T \varphi_{k+1}^{(k)}\right)}, \quad k = 0, \ldots, n-1 \tag{8}$$

The derivation details can be found from (Li and Peng, 2005). Eq. (8) shows the net contribution of term φ_{k+1} to the cost function when it is included in the model.

In order to simplify the computational complexity, two quantities are denoted as

$$\begin{cases} a_{k,i} \triangleq \left(\varphi_k^{(k-1)}\right)^T \varphi_k^{k-1} a_{1,i} \triangleq \varphi_1^T \varphi_i, i = k, \ldots, n \\ a_{k,y} \triangleq \left(\varphi_k^{(k-1)}\right)^T y a_{1,y} \triangleq \left(\varphi_1^0\right)^T y = \varphi_1^T y, k = 1, 2, \ldots, n \end{cases} \tag{9}$$

We can define an auxiliary matrix $a \in R^{n \times n}$ and a vector $b \in R^{n \times n}$ with the elements given by

$$\begin{cases} a_{k,i} = \varphi_k^T p_i - \frac{\sum_{j=1}^{k-1}\left(a_{j,k} a_{j,i}\right)}{a_{j,j}}, & k = 1, \ldots, n \\ a_{k,y} = \varphi_k^T y - \frac{\sum_{j=1}^{k-1}\left(a_{j,k}, a_{j,y}\right)}{a_{j,j}}, & i = k, \ldots, n \end{cases} \tag{10}$$

Then the net contribution of $\varphi_{k+1}, k = 0, 1, \ldots, n-1$ to the cost function can be shown explicitly as following

$$\Delta E_{k+1} = -\frac{\left(y^T \varphi_{k+1} - \sum_{j=1}^{k}\left(\frac{a_{j,y} a_{j,k+1}}{a_{j,j}}\right)\right)^2}{\left(\varphi_{k+1}\right)^T \varphi_{k+1} - \sum_{j=1}^{k}\left(\frac{a_{j,k+1}^2}{a_{j,j}}\right)} \tag{11}$$

Equation (11) gives the fast algorithm for explicitly computing the net contribution of a selected model term. After selecting the model terms, the model parameter can be computed recursively using

$$\widehat{\theta}_j = \frac{\left(a_{j,y} - \sum_{i=j+1}^{k} \widehat{\theta}_i a_{j,i}\right)}{a_{j,j}}, j = k, k-1, \ldots, 1 \tag{12}$$

Table 1. Summary of the nonlinear extended Kalman filter (Plett, G. L., 2015).

Nonlinear state-space model:

$\boldsymbol{x}_k = \boldsymbol{f}(\boldsymbol{x}_{k-1}, \boldsymbol{u}_{k-1}, \boldsymbol{w}_{k-1})$

$\boldsymbol{y}_k = \boldsymbol{h}(\boldsymbol{x}_k, \boldsymbol{u}_k, \boldsymbol{v}_k)$

where w_k and v_k are independent, Gaussian noise processes with means $\bar{w}$ and $\bar{v}$ and covariance matrices $\Sigma_{\tilde{w}}$ and $\Sigma_{\tilde{v}}$, respectively.

Definitions:

$\hat{A}_k = \left.\frac{df(x_k,u_k,w_k)}{dx_k}\right|_{x_k=\hat{x}_k^+}$ $\hat{\boldsymbol{B}}_k = \left.\frac{df(x_k,u_k,w_k)}{dw_k}\right|_{w_k=\bar{w}_k}$

$\hat{C}_k = \left.\frac{dh(x_k,u_k,v_k)}{dx_k}\right|_{x_k=\hat{x}_k^-}$ $\hat{\boldsymbol{D}}_k = \left.\frac{dh(x_k,u_k,v_k)}{dv_k}\right|_{v_k=\bar{v}_k}$

Initialization: For k=0 , set

$\hat{x}_0^+ = \mathbb{E}[x_0]$

$\Sigma_{\tilde{x},0}^+ = \mathbb{E}\left[\left(x_0 - \hat{x}_0^+\right)\left(x_0 - \hat{x}_0^+\right)^T\right]$.

Computation: For $k = 1, 2, \ldots$ compute:

State-prediction time update: $\hat{x}_k^- = f\left(\hat{x}_{k-1}^+, \boldsymbol{u}_{k-1}, \overline{\boldsymbol{w}}_{k-1}\right)$

Error-covariance time update: $\Sigma_{\tilde{x},k}^- = \hat{A}_{k-1}\Sigma_{\tilde{x},k-1}^+\hat{A}_{k-1}^T + \hat{\mathbf{B}}_{k-1}\Sigma_{\tilde{w}}\hat{\boldsymbol{B}}_{y-1}^T$

Output estimate: $\hat{y}_k = \boldsymbol{h}\left(\hat{x}_k^-, \boldsymbol{u}_k, \bar{v}_k\right)$

*Estimator gain matrix:** $\boldsymbol{L}_k = \boldsymbol{\Sigma}_{\tilde{\boldsymbol{x}},k}^-\hat{\boldsymbol{C}}_k^T\left[\hat{\boldsymbol{C}}_k\boldsymbol{\Sigma}_{\tilde{\boldsymbol{x}},k}^-\hat{\boldsymbol{C}}_k^T + \hat{\boldsymbol{D}}_k\boldsymbol{\Sigma}_{\tilde{\boldsymbol{v}}}\hat{\boldsymbol{D}}_k^T\right]^{-1}$

State-estimate meas. update: $\hat{x}_k^+ = \hat{x}_k^- + L_k(y_k - \hat{y}_k)$

Error -covariance meas. update: $\boldsymbol{\Sigma}_{\tilde{\boldsymbol{x}},k}^+ = \boldsymbol{\Sigma}_{\tilde{\boldsymbol{x}},k}^- - \boldsymbol{L}_k\boldsymbol{\Sigma}_{\tilde{\boldsymbol{y}},k}\boldsymbol{L}_k^T$

2.2. Extended Kalman Filter

The EKF uses a linearization process at each time step k to approximate the nonlinear system. The main procedure of EKF is illustrated in Table 1.

2.3. Model Evaluation Criteria

To evaluate the performance of the constructed models, two distinct performance metrics are utilized (Liu and Li, 2023). The first metric is the mean squared error (MSE) used for assess the accuracy of the estimated values. The MSE is defined as

$$\text{MSE} = \frac{1}{n}\sum_{i=1}^{n}\left(Y_i - \hat{Y}_i\right)^2 \tag{13}$$

where Y_i is the actual value and $\hat{Y}_i$ are the estimation value. n denotes the number of data samples used for model training/testing.

The second evaluative metric employed is the Mean Absolute Error (MAE). This is computed as the aggregate of absolute discrepancies between observed and predicted values, normalized by the total quantity of instances utilized during the model training or testing phase

$$MAE = \frac{\sum_{i=1}^{n}\left|Y_i - \hat{Y}_i\right|}{n} \tag{14}$$

where Y_i is the true value and $\hat{Y}_i$ is the prediction. n is the number of data samples used for modeling.

3. Experimental setup

3.1. Experimental bench

Two commercial rechargeable Li-ion Polymer Batteries (GPR 6742126-35C-3.2V, 2500mAh) are serially connected to compose a representative battery pack. The details of the battery pack and its associated cells are provided in Table 2. During the experiment, the strain and temperature signals of each battery cell were continuously monitored by an optical fibre sensing network, as shown in Fig. 3.1. The optical fibre sensing network comprises two fibres of the same type. Each fibre contains two Fibre Bragg Gratings (FBGs), with FBG1 and FBG2 located in the first fibre and FBG3 and FBG4 in the second fibre. These four FBG sensors are sensitive to both strain and temperature variations. However, when the FBG sensor is loosely attached to the cell skin with a thermal-conducting paste, it becomes sensitive only to temperature variations (Han et al., 2021). During the experiment, FBG1 and FBG2 were glued to the surface of the two batteries using Cyano adhesive to monitor temperature and strain variations simultaneously. FBG3 and FBG4 were placed loosely on both sides of FBG1 and FBG2 to measure temperature variations in those two locations. The central wavelength for each FBG sensor was 1538 nm, 1545 nm, 1536 nm, and 1546 nm respectively. Furthermore, two K-type thermocouples were glued to the selected locations on the batteries to read temperatures that served as references. Thermal paste was placed along all fibres to increase thermal conductivity between the batteries and the FBGs.

Table 2. Properties of battery cell and battery pack.

Battery properties	Parameters
Nominal Voltage	6.4 V
Nominal Capacity	2500 mAh
Pack Arrangement	2 cells serial-connected
Cell cut-off voltage	2.0 V, 3.65 V
Standard Charging Current	500 mA
Standard Discharging Current	500 mA
Rapid Charge current	2500 mA
Max. Constant Discharge Current	87500 mA

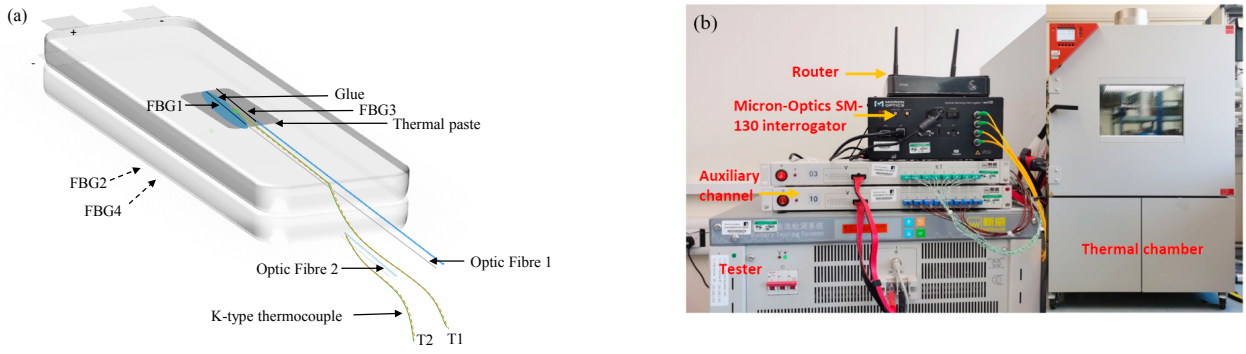

Fig. 1. (a) Schematic of the battery pack, and (b) the test bench

A NEWARE BTS4000 (60V,100A) battery tester was used to control and acquire the battery pack terminal voltage and pack current during the tests. The auxiliary channel was also used to collect the voltage and temperature of each cell. The tests were performed inside a BINDER (LIT MK 240) battery test chamber to maintain and adjust the ambient temperature at 23°C. The host computer with the installed BTS-7.5 software was used to program the test procedure and store the test data. The sampling frequency for all tests conducted in the study was set to 1 Hz.

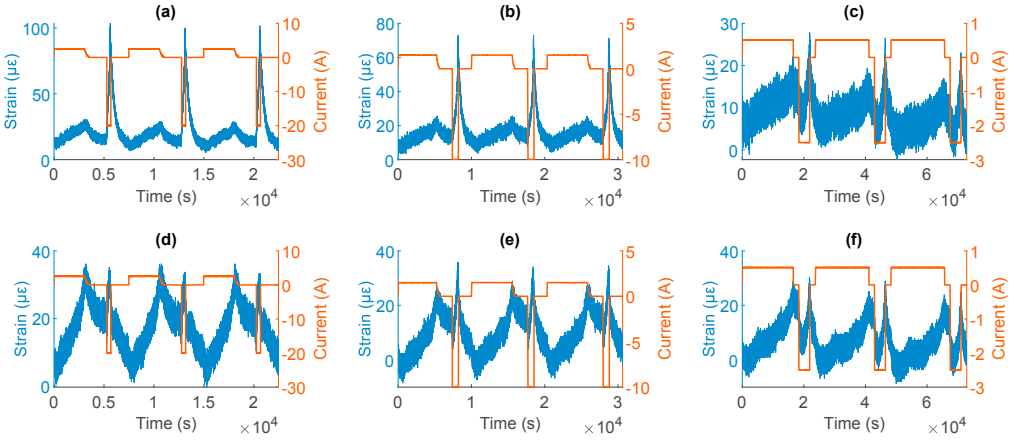

Fig. 2. Illustration of the current profile along with the strain response; (a), (b), (c) are cell#1 charging/discharging process, (d), (e), (f) are cell#2 charging/discharging process.

3.2. Data collection

The standard cycle profiles, including different Constant-Current Constant-Voltage (CC-CV) charging processes and different Constant-Current (CC) discharging processes, were applied to the battery pack in the experiment. Specifically, the pack was charged under 1C, 0.6C, and 0.2C, respectively, until the terminal voltage of any cell reached the upper cut-off voltage (3.65 V). Then the pack was charged under the constant voltage until the charging current decreased to 65 mA. For the CC discharging process, the corresponding currents 1C, 4C, and 8C were applied to the battery pack, respectively, until any cell reached a lower cut-off voltage of 2.0V. The rest time between each charging and discharging process is set to 10 minutes.

3.3. Cell surface strain analysis

The battery cell surface strain variations, along with the charging current, are illustrated in Fig. 2. It can be observed that the strain response of the two series-connected batteries is significantly different under the same working current. For cell#1 (as shown in Fig. 2(a), (b), and (c)), its strain value obviously varies under different charging and discharging currents. On the other hand, for cell#2 (as shown in Fig. 2(d), (e), and (f)), its strain signal also shows some kind of correlation with the current, but its variations remain largely unchanged under different charging or discharging currents.

Albeit the differences between the two cells, it is evident that the surface strain of both batteries increased during the charging and discharging processes and began to decrease once the batteries were at the resting phase. Moreover, the strain exhibited a consistent trend during three consecutive charging and discharging cycles. These results indicate that surface strain measurements could be used to model the correlations between the strain signal and other states for each individual cells.

4. Model construction for battery pack SOC estimation

4.1. Battery pack SOC calculation

In this work, we propose to integrate two strategies to estimate the SOC of the battery pack. In the first strategy, the battery pack SOC is initially calculated based on the SOC of each cell and then identified as the representative SOC value on the charging and discharging process. During the charging process, the battery pack SOC is determined by the highest SOC value for both cells. Conversely, during discharge, it is represented by the lowest SOC value among all cells.

During the charging process, the cell-based SOC results can be represented as

$$SOC_{\text{cell}(t)} = \text{Max}\left(z_{1(t)}, z_{2(t)}, \ldots, z_{n(t)}\right) \tag{15}$$

Upon the discharging process, the cell-based SOC results are calculated

$$SOC_{\text{cell}(t)} = \text{Min}\left(z_{1(t)}, z_{2(t)}, \ldots, z_{n(t)}\right) \tag{16}$$

where $z_n, (n = 1, 2, \ldots k)$ represents the *nth* series-connected cell SOC in a battery pack. $SOC_{\text{cell}(t)}$ is the battery pack SOC at time t based on the cell strategy.

The second strategy is to consider the battery pack as a "big cell". Then an equivalent circuit model is employed in conjunction with the EKF to obtain the overall SOC (named, $SOC_{\text{pack}(t)}$) for the entire battery pack.

The final SOC value of the battery pack is calculated by averaging the results obtained from the cell-based strategy and pack-based strategy:

$$SOC_{\text{final }(t)} = \frac{SOC_{\text{cell }(t)} + SOC_{\text{pack }(t)}}{2} \tag{17}$$

The models for cell-based and pack-based SOC estimation will be introduced in the subsequent sections.

4.2. Strain-based battery cell SOC estimation approach

To calculate the SOC value of each cell, we used the FRA approach to build a correlation model between the battery electrical parameters and surface strain. FRA is capable of quickly selecting the most significant ones from a large pool of candidate model terms avoiding overfitting and underfitting. Based on the selected model terms, FRA can also quickly identify the model coefficients.

The detailed procedure to determine the significant terms and corresponding weights of nonlinear models is shown as follows:

1. Generating the candidate model term pool which contains the battery pack parameters: Current (i), Voltage (v), temperature (T), SOC (z), as well as the nonlinear forms corresponding to each feature, such as exponential form, logarithmic form, and trigonometric form, etc.
2. Calculating the net contribution of model terms and selecting the largest contributors using Eq. (11).
3. Repeat the selection step until the SSE criterion is achieved.
4. After selecting the appropriate model terms, calculate the model parameters using Eq. (12).

4.2.1. Model construction based on FRA

It is worth noting that for the same FBG sensors, the trajectories of the measured strain are significantly different during the charging and discharging process since the electrochemical reactions inside the battery during the charging and discharging are different. Thus, the relationship between the SOC and the measured strain signals is different for the charging and discharging processes. It is therefore reasonable to model the relationship between the SOC and the measured strain signals separately for the charging and discharging processes.

For cell#1, the measured strain signal can be expressed as a function of the input current, temperature, and SOC:

$$\begin{aligned}\varepsilon^1_{Ck} =& -1.1645 * 10^{-12} T_k^{10} + 0.0198 z_k^2 - 8.8824 * 10^{-40} e^{z_k} + 3.1764 * 10^{-11} T_k^9 - 0.308 z_k \\ &+ 5.7510 * 10^{-41} \left(e^{i_k}\right)^2 e^{z_k} + 3.5580 * 10^{-20} i_k z_k^{10} - 3.0751 * 10^{-4} z_k^3 + 1.5519 * 10^{-6} z_k^4\end{aligned} \tag{18}$$

$$\begin{aligned}\varepsilon^1_{Dk} =& 0.0075 T_k^3 + 4.0654 * 10^{-13} \left(i_k^8\right)\left(z_k^3\right) + 4.5673 * 10^{-13} T_k^{10} + 0.0192 \left(i_k^2\right) z_k \\ &+ 8.4305 * 10^{-20} \left(i_k^7\right)\left(z_k^7\right) - 1.9360 * 10^{-11} T_k^9 + 4.5253 * 10^{-16} \left(i_k^6\right)\left(z_k^6\right) \\ &+ 4.2115 * 10^{-10} \left(i_k^7\right)\left(z_k^2\right) - 3.7575 * 10^{-14} \left(i_k^6\right)\left(z_k^5\right)\end{aligned} \tag{19}$$

where ε^1_{Ck} and ε^1_{Dk} represent the strain changes during the charging and discharging processes for cell#1, respectively. And i_k, z_k and T_k are current, SOC, and temperature at time step k.

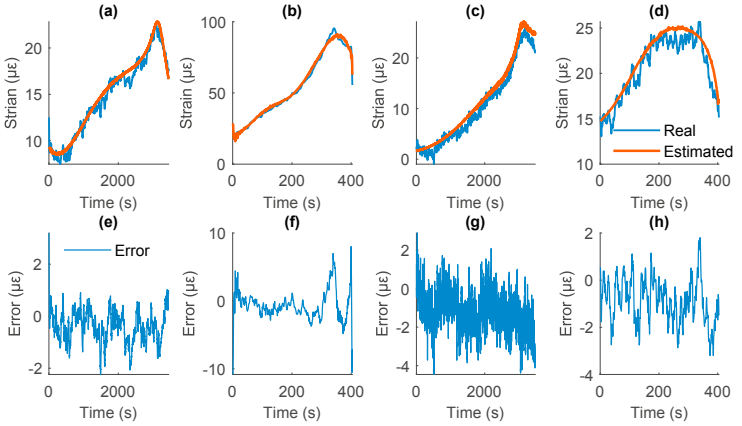

Fig. 3. Validation of the battery cell strain model. (a) Comparison of real and estimated strain values during the charging process of cell#1. (b) Comparison of real and estimated strain values during the discharging process of cell#1. (c) Comparison of real and estimated strain values during the charging process of cell#2. (d) Comparison of real and estimated strain values during the discharging process of cell#2. Figures (e), (f), (g), and (h) correspond to the estimation error for figures (a), (b), (c), and (d), respectively.

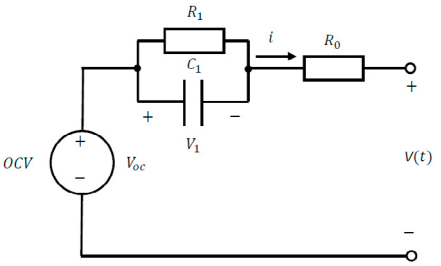

Fig. 4. First-order equipment circuit model.

Similarly, for cell#2, the function expressing strain in relation to current, SOC, and temperature can be defined as follows.

$$\begin{aligned}\varepsilon^2_{Ck} = {} & 8.1954 * 10^{-9}\left(T_k^4\right)\left(z_k^2\right) + 2.6971\sin\left(i_k\right) + 6.0305 * 10^{-19} z_k^{10} + 0.0086 i_k z_k \\ & - 5.2365 * 10^{-10}\left(T_k^2\right)\left(z_k^4\right) + 1.1758 * 10^{-4}\left(i_k^2\right)\left(z_k^2\right)\end{aligned} \tag{20}$$

$$\begin{aligned}\varepsilon^2_{Dk} = {} & 0.0058 i_k T_k + 7.8754 * 10^{-16}\left(T_k^8\right)\left(z_k^2\right) + 7.4827 * 10^{-17}\left(T_k^8\right)\left(z_k^3\right) \\ & - 1.2811 * 10^{-18}\left(T_k^8\right)\left(z_k^4\right) + 0.8389 T_k - 9.7543 * 10^{-16} T_k^{10}\end{aligned} \tag{21}$$

where ε^2_{Ck} and ε^2_{Dk},represent the strain changes in cell#2 during the charging and discharging processes, respectively. i_k, z_k and T_k are current, SOC, and temperature at time step k, respectively.

4.2.2. Model valiation

To evaluate the constructed models, another set of data was used. The corresponding strain values were then compared with the predictions. Fig. 3 illustrates the comparison between the actual strain values and the estimated ones. The MSEs for the charging and discharging processes of cell#1 are 2.95% and 0.93%, respectively. In the case of cell#2, the MSEs for the charging and discharging processes are 4.20% and 14.80%, respectively.

4.2.3. Application of EKF

In this work, the battery cell SOC is defined as the ratio of the available capacity to the nominal capacity of the battery. The definition can be given by

$$z(t) = z(t_0) - \frac{1}{Q}\int_{t_0}^{t} \eta(t) i(t) \mathrm{d}t \tag{22}$$

where $z(t)$ and $z(t_0)$ are the SOC values at the time t and the initial moment t_0, respectively, η_t is the coulombic efficiency reflecting the ratio of the fully discharged energy to the charged energy required to restore the original capacity (Hu et al., 2019). The current $i(t)$ is assumed to be positive for charging and negative for discharging. Q represents the maximum available capacity of the battery. This expression is known as the Ampere-hour (Ah) integral method.

The discrete-time expression for the relationship is presented in Eq. (23).

$$z_{k+1} = z_k - \eta_k \frac{\Delta t}{Q} (i_k + w_k) \tag{23}$$

Δt represents the sampling period, and η_k is the coulombic efficiency.

In order to utilize the strain value for battery cell SOC estimation, the constructed state-space model, which includes both the state and measurement functions, is demonstrated in Eq. (24).

$$\begin{cases} z_{k+1} = f(z_k, i_k, w_k) \\ \varepsilon_{k+1} = h(z_{k+1}, i_{k+1}, T_{k+1}, v_{k+1}) \end{cases} \tag{24}$$

where z_{k+1} and z_k represent the SOC at time $k+1$ and k, respectively. i_k represents the current at time k, while ε_{k+1} is the strain value at time $k+1$.w_k and v_{k+1} indicate the current and strain measurement error, respectively. And T_{k+1} denotes temperature at time $k+1$. This state function suggests that the observed strain is determined by SOC, charging/discharging current and temperature.

4.3. Thevenin model-based Battery pack SOC estimation approach

In the work, a first-order Equivalent Circuit Model (ECM, also named Thevenin model) was built for the battery pack (i.e. consider the battery pack as a "big cell"), as shown in Fig. 4. This model consists of a voltage source V_{oc}, an ohmic resistance R_0, and the RC network (R_1 and C_1) to describe the polarization effects and dynamic voltage performance in the circuit. Here, i represents the load current with positive values indicating discharging and negative values indicating charging. Moreover, V_1 denotes the voltage across the RC network, while V_t represents the voltage at the battery terminal.

The first-order equivalent circuit can be expressed by

$$\begin{cases} \dot{V}_t = -\frac{1}{R_1 C_1} v_1 + \frac{1}{C_1} i \\ V_t = V_{OC} - v_1 - i R_0 \end{cases} \tag{25}$$

Assuming that the sampling time is ΔT, the discretizing Equations can be expressed as follows:

$$\begin{cases} V_{1,k} = V_{1,k-1} \exp(-\Delta T/\tau) + [1 - \exp(-\Delta T/\tau)] R_1 i_k \\ V_{t,k} = V_{oc,k} - V_{1,k} - i_k R_1 \end{cases} \tag{26}$$

where $\tau = R_1 C_1$, and k denotes the step of discrete time series with the sampling period ΔT, $k = 1, 2, 3, \ldots$

5. Results and discussions

The estimation results based on the aforementioned models are displayed in Fig. 5. Fig. 5(a) is the charging process whereas Fig. 5(b) illustrates the discharging process. It is evident from the figures that both the strain-based method and the ECM-based method can yield accurate SOC results. However, the strain-based model exhibits larger fluctuations during the discharging phase when compared to the equivalent circuit model estimation results.

Fig. 5(c) and (d) present a comparison of results from the strain-based method, ECM method, and joint method alongside the Ah integral method, respectively. Here, the reference value is calculated based on the Ah integral method. Calculations reveal that during the charging process, the MSE and MAE of the first-order equivalent circuit model are 2.19% and 1.28%, respectively. For the discharging process, the MSE and MAE are 3.03% and 1.39%, respectively. In contrast, the MSE for the strain model during the charging and discharging processes are 3.96% and 35.94%, respectively. The MAE for the strain model during these processes are 1.64% and 4.48%, respectively.

Finally, during the charging process, the MSE and MAE for the joint method are 1.89% and 1.18%, respectively; the MSE and MAE for the discharging process are 6.45% and 1.82%, respectively. Obviously, it performs best among all models with the lowest MSE and MAE values during the charging process compared to the single strain method or equivalent circuit model for estimating the battery pack SOC.

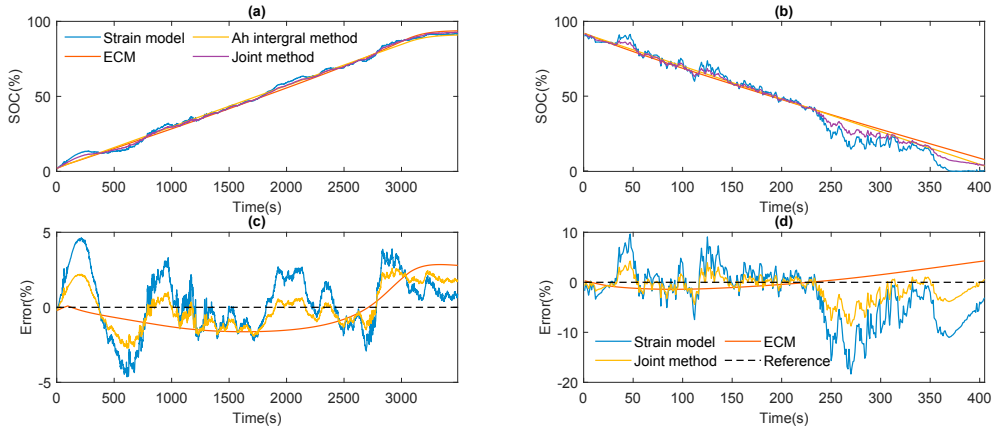

Fig. 5. SOC estimation result and the estimation error; (a) charging phase SOC, (b) discharging phase SOC, (c) charging phase SOC error, (d) discharging phase SOC error.

Although the joint method shows a higher MSE and MAE during the discharging process, its overall performance is notable. For example, observations from Fig. 5(c) and (d) indicate that at certain time steps when one model's error is high, the other model often shows lower errors. This complementary performance suggests that the joint method can effectively balance the weaknesses of the individual models, providing a more robust and reliable estimation SOC of the battery pack.

6. Conclusion

This paper presents a joint battery pack SOC estimation approach based on both the single-cell approach and the big-cell approach. First, a fibre optical sensor network is installed to monitor the strain and temperature variations on each individual cell, and a strain model is then built for SOC estimation at the cell level. Then, an equivalent circuit model is developed for the entire battery pack, using the single "big cell" approach for battery pack SOC estimation. The final battery pack SOC value is calculated by taking the average of the results from the two models. The joint model offers the advantage of reducing the impact caused by the corruptions even failures of either electrical signals or the fibre optical signals, resulting in more accurate and reliable estimation. Future work will focus on multi-state estimation based on the joint strategy.

References

Yu, Q., Huang, Y., Tang, A., Wang, C., Shen, W., 2023. OCV-SOC-Temperature Relationship Construction and State of Charge Estimation for a Series–Parallel Lithium-Ion Battery Pack. IEEE Transactions on Intelligent Transportation Systems.

Hua, Y., Cordoba-Arenas, A., Warner, N., Rizzoni, G., 2015. A multi time-scale state-of-charge and state-of-health estimation framework using nonlinear predictive filter for lithium-ion battery pack with passive balance control. Journal of Power Sources 280, 293-312.

Dai, H., Wei, X., Sun, Z., Wang, J. and Gu, W., 2012. Online cell SOC estimation of Li-ion battery packs using a dual time-scale Kalman filtering for EV applications. Applied Energy 95, 227-237.

Li, K., Peng, J-X., G. W., 2005. A fast nonlinear model identification method. IEEE Transactions on Automatic Control 50.8, 1211-6.

Li, Y., Li, K., Liu, X., Wang, Y., Zhang, L., 2021. Lithium-ion battery capacity estimation — A pruned convolutional neural network approach assisted with transfer learning. Applied Energy 285.

Plett, G. L., 2015. Battery management systems, Volume II: Equivalent-circuit methods. Artech House.

Liu, S., Li, K., 2023. Thermal monitoring of lithium-ion batteries based on machine learning and fibre Bragg grating sensors. Transactions of the Institute of Measurement and Control.

Han, G., Yan, J., Guo, Z., Greenwood, D., Marco, J., Yu, Y., 2021. A review on various optical fibre sensing methods for batteries. Renewable and Sustainable Energy Reviews 150, 111514.

Hu, X., Feng, F., Liu, K., Zhang, L., Xie, J., Liu, B., 2019. State estimation for advanced battery management: Key challenges and future trends. Renewable and Sustainable Energy Reviews 114, 109334.